An estimate of the stratospheric input to the troposphere during TOPSE using ^{7}Be measurements and model simulations

Dale Allen (Department of Meteorology, University of Maryland)

Jack Dibb (Institute for the Study of Earth, Oceans, and Space, University of New Hampshire)

Kenneth Pickering (Department of Meteorology, University of Maryland)

Brian Ridley (Atmospheric Chemistry Division, National Center for Atmospheric Research)

Submitted to J. Geophys. Res.

25 October 2001

Abstract. The distribution of ^{7}Be during the TOPSE period was simulated using a global model driven by data from the Goddard Earth Observing System Data Assimilation System (GEOS−3 DAS). Temporal changes in the stratospheric component of tropospheric air were analyzed using model output and ^{7}Be measurements. Comparison of model−calculated ^{7}Be concentrations in the lower and upper troposphere with measurements revealed that cross tropopause exchange of ^{7}Be was overestimated by only 10−25%. This bias is much less than what was seen in calculations with a different vertical grid driven by earlier versions of the GEOS DAS. The location and timing of fluctuations in ^{7}Be concentrations were well captured by the model even during constant altitude portions of TOPSE flights. The amplitudes of the fluctuations were often underestimated. Within the TOPSE region (100°−60°W, 40°−80°N), 55−60% of ^{7}Be in the model troposphere had a stratospheric source. No significant temporal trend is evident in observed or model−calculated ^{7}Be concentrations. Model−calculated mean tropospheric ^{7}Be concentrations increased by 2.9% per month in the southern portion of the TOPSE region. The stratospheric component in this region increased by only 0.6% per month. Analysis of the ^{7}Be budget shows that seasonal increases in STE and scavenging contribute to this increase. Tropospheric O_3 increases resulting from this increase are likely to be less than 1% per month. Model−calculated mean tropospheric ^{7}Be concentrations increased by 1.6% per month in the northern portion of the TOPSE region. Analysis of the ^{7}Be budget showed that seasonal increases in STE did not contribute to this increase.

1. Introduction

Measurements of tropospheric ozone (O_3) show springtime maxima in the troposphere at remote locations of the northern midlatitudes [*Oltmans*, 1981; *Logan*, 1985]. Seasonal changes in photochemistry [*Penkett and Brice*, 1986] and/or stratosphere−troposphere exchange (STE) [*Bazhanov and Rodhe*, 1997] may contribute to these maxima. O_3 concentrations in the lower stratosphere typically exceed upper tropospheric concentrations by at least an order of magnitude. O_3 and potential vorticity are positively correlated in the middle and upper troposphere during upper level baroclinic events [*Danielson*, 1968] indicating that the stratosphere is a source for middle and upper tropospheric O_3. It is unclear if this stratospheric source increases with time during the spring. The frequency of tropopause folds does not appear to peak in the northern hemisphere spring [*Holton et al.*, 1995; *Postel and Hitchman*, 1999]; although, the cross tropopause mass flux associated with these folds is large during December−June and peaks during late spring [*Appenzeller et al.*, 1996]. Since the lifetime of O_3 is about a month in the troposphere, a peak in tropospheric O_3 due to this increased flux is also likely during this period [*Logan*, 1985]. Synoptic conditions following STE are conducive to large−scale subsidence that transports this O_3 from the upper to the lower troposphere [*Moody et al.*, 1996; *Cooper et al.*, 1998].

An understanding of the processes contributing to these maxima is a major goal of the Tropospheric Ozone Production about the Spring Equinox Experiment (TOPSE). In this study, seasonal changes in the stratospheric component of tropospheric air are evaluated using Beryllium−7 (^{7}Be) data and model output. The focus of the study is the TOPSE region (defined here to be 100°−60°W, 40°−80°N) and period (defined here to be February 1 − May 31, 2000).

2. Motivation: Why simulate ^{7}Be?

The radionucleide ^{7}Be is a chemically non−reactive passive tracer generated when neutrons created by collisions between primary cosmic rays and atoms collide with nitrogen and oxygen atoms. Since cosmic rays follow the Earth's magnetic field, ^{7}Be production is largest at high−latitudes. ^{7}Be is often used as a tracer of stratospheric air [*Husain et al.*, 1977] because its production is largest in the stratosphere and its loss (radioactive decay with a half−life of 53 days and scavenging by precipitation) is largest in the troposphere. The combination of high stratospheric production rates and rapid tropospheric removal results in stratospheric ^{7}Be concentrations exceeding tropospheric concentrations by about an order of magnitude [e.g., *Dutkiewicz and Husain*, 1985]. Consequently, ^{7}Be is a sensitive indicator of STE. Considerable STE occurs during tropopause folds. *Viezee and Singh* [1980] discovered that seasonal and latitudinal variations in tropospheric ^{7}Be concentrations and in the frequency of occurrence of 500−hPa low−pressure troughs are highly correlated over the continental United States. *Dibb et al.* [1992] attributed a mid−tropospheric peak in ^{7}Be concentrations in the Arctic to injection of stratospheric air through tropopause folds. Seasonal changes in stratospheric influence in the Arctic have also been studied using beryllium isotope ratios. *Dibb et al.* [1994] attributed spring maxima in surface layer concentrations of ^{7}Be and ^{10}Be to seasonal changes in vertical mixing within the troposphere rather than seasonal changes in STE.

Modeling studies have used ^{7}Be as a tool to evaluate transport, especially stratospheric input to the troposphere [*Rehfeld and Heimann*, 1995; *Koch and Rind*, 1998] and scavenging parameterizations [*Brost et al.*, 1991; *Koch et al.*, 1996; *Liu et al.*, 2001]

3. Description

3.1. ^{7}Be and O_3 data

Dibb et al. [this issue] describe the procedure used to determine ^{7}Be activities during the TOPSE mission. Atmospheric aerosol samples were collected on filters during 12−24 minute constant altitude sampling periods. The filters were shipped to a laboratory and analyzed for ^{7}Be activity using gamma spectroscopy. Activities were adjusted for loss by decay during the time period between sampling and analysis. Beryllium−7 concentrations from 298 samples collected during TOPSE flights 5−42 are used in this study. Beryllium−7 concentrations from 239 of these samples exceeded the detection limit. Detection limits (0.8 to 4.5 mBq / SCM) varied with sampling pressure and time. Concentrations less than the detection limit were set to the detection limit. The maximum concentration was175 mBq / SCM while the mean and median concentrations were 20.0 and 11.4 mBq / SCM, respectively. The standard deviation was 26.7 mBq / SCM.

Five−minute average O_3 data are also used in this paper. These data are part of 300−second TOPSE data merges available through the National Center for Atmospheric Research Atmospheric Chemistry Division (NCAR ACD). The method used to collect the O_3 data used in the merges is described in *Ridley et al.* [this issue].

3.2. University of Maryland CTM

The distribution of ^{7}Be was simulated using the University of Maryland chemistry and transport model (UMD−CTM), a version of the Goddard CTM [*Allen et al.*, 1996a,b] that includes wet scavenging and dry deposition. The calculations were driven by data from version

3 of The Goddard Earth Observing System Data Assimilation System (GEOS−3 DAS) [*Schubert et al.*, 1993; *Bloom et al.*, 1996]. The mixing ratio change due to advection is calculated using a multidimensional and semi−Lagrangian extension of the piecewise parabolic method (PPM) [*Lin and Rood*, 1996]. Convective mixing in the UMD−CTM [*Allen et al*., 1996b] is calculated using cumulus mass flux and detrainment output from the Relaxed Arakawa−Schubert (RAS) algorithm [*Moorthi and Suarez*, 1992; *Arakawa and Schubert*, 1974] that is used to parameterize convection in the GEOS GCM. Three−hour averaged planetary boundary layer depths are available from the GEOS−3 DAS. Turbulent mixing within the boundary layer is parameterized using a fractional mixing scheme [*Allen et al*, 1996a]. Dry deposition is parameterized based on surface type [e.g., *Brasseur et al.*, 1998] with deposition velocities from *Sander and Crutzen* [1996]. Wet removal of soluble species is accomplished through a wet scavenging algorithm described in *Chin et al.* [2000] using precipitation rates from the GEOS−3 DAS. Scavenging by cirrus precipitation [*Lawrence and Crutzen*, 1998; *Liu et al*., 2001] is not included.

Data from the GEOS−3 DAS are archived on a 48−sigma layer 1° in latitude by 1° in longitude (1° x 1°) grid. The UMD−CTM was run at a 2° x 2.5° resolution with 35 sigma−pressure layers. The model tops of the GEOS−3 DAS and the UMD−CTM are 0.01 hPa. Pressures at the tops and bottoms of the first 25 GEOS−3 DAS and UMD−CTM layers (~1000 hPa to ~37.6 hPa) are identical. The uppermost 23 GEOS−3 DAS layers are mapped onto 10 UMD−CTM layers. The resulting fields are mapped onto a 2° x 2.5° grid. The UMD−CTM grid includes 8 layers between the surface and 850 hPa and 13 layers between 850 hPa and 100 hPa with a vertical resolution in the expected TOPSE tropopause region of 1.4 to 1.8 km. The sigma−pressure interface of the UMD−CTM is ~242 hPa. Six−hour averaged *u* and *v* components of the wind are taken from the GEOS−3 DAS. The winds are interpolated in time

to the transport time. The vertical velocity is calculated kinematically each transport time step (15 minutes) by assuming the vertical velocity is zero at the top of the model and integrating downward.

3.3. ^{7}Be calculations

Beryllium−7 production varies with the solar cycle. It is smallest when the solar cycle is near its maximum and largest when the cycle is near its minimum. The solar cycle was near its maximum in 2000. The ^{7}Be source used in this study, 0.080 atoms ^{7}Be m^{-2} s^{-1}, [*Lal and Peters*, 1967] is appropriate for a solar maximum year. Following *Liu et al.* [2001], we divided the ^{7}Be source into tropospheric and stratospheric components using the tropopause pressure. The tropopause pressure was calculated for each grid point in the GEOS−3 DAS. It is defined to be the largest GEOS−3 DAS pressure (pressure < 600 hPa) at which the Ertel potential vorticity equals 2.5 x 10^{-6} K m^{2} $kg^{-1}s^{-1}$. However, if the resulting tropopause pressure is less than the pressure at the 380 K surface, the pressure at the 380 K surface is used as the tropopause pressure. Calculations began 1 Jan 2000 following a 6−month spin up from an initial condition of ^{7}Be = 0 using GEOS−3 DAS fields from July − December 2000. The GEOS−3 assimilation did not begin until November 1999.

The time−averaged (February 1 − May 31, 2000) ^{7}Be budget for the globe is shown in Table 1. Seventy−one percent of model−calculated ^{7}Be is produced in the stratosphere. This value agrees well with the value (70%) given in *Lal* [1963] and *Lal and Peters* [1967]. Radioactive decay is the dominant loss mechanism for ^{7}Be with a stratospheric source (strat−^{7}Be), while wet scavenging is the dominant loss mechanism for ^{7}Be with a tropospheric source (trop−^{7}Be). Dry deposition plays a relatively minor role. The time−averaged ^{7}Be budget for the

TOPSE region is also shown in Table 1. In this region, because of the relatively low tropopause, strat−^{7}Be accounts for 84% of the total ^{7}Be production. The relative importance of radioactive decay is also enhanced primarily due to low scavenging rates over the northern portion of the TOPSE region.

The zonally averaged model−calculated ^{7}Be distribution in mBq/SCM (see appendix) and its stratospheric component (strat−^{7}Be/ total−^{7}Be) are shown for the TOPSE period in Figures 1a−b. As expected, stratospheric concentrations exceed tropospheric concentrations by nearly an order of magnitude. At a given pressure within the troposphere, concentrations are largest in the descending branches of the Hadley circulation and lowest at latitudes where scavenging is large. In general, model−calculated concentrations are similar to concentrations shown by *Liu et al*. [2001] for a simulation without cirrus scavenging. The magnitude of ascent and descent within the Hadley circulation is less than that shown by *Liu et al.* [2001]. The stratospheric component in the troposphere varies from 15−80%. Lowest values are found in the mid−troposphere at equatorial locations and near the surface at polar locations.

4. Comparison of model−calculated and observed ^{7}Be

4.1. Mean distributions

Beryllium−7 was sampled on 31 days during 38 TOPSE flights. Mean ^{7}Be concentrations during each of these days are shown with asterisks in Figure 2. Mean concentrations for each of these days were calculated by weighting individual measurements by sampling times. The contributions from trop−^{7}Be and strat−^{7}Be are shown with diagonal and horizontal lines, respectively. Mean model−calculated concentrations for each day were

calculated by weighting model output interpolated to the locations (longitude, latitude, and pressure) and times of ^{7}Be measurements by the sampling period. Mean ^{7}Be sampling pressures (P) and GEOS−3 DAS tropopause pressures (T) are also shown for each of the flight dates. Nearly all measurements were taken at pressures greater than the GEOS−3 tropopause pressure. Two hundred−and−ninety of the 298 samples had sampling pressures more than 10 hPa greater than the model−calculated tropopause pressure. Mean model−calculated concentrations exceeded mean measured concentrations by only 5%.

Observed daily−average ^{7}Be concentrations in the upper troposphere exceeded 30 mBq/SCM on March 7, April 2, April 28, and April 30. Model−calculated concentrations on March 7, April 2, and April 28 also exceeded this value. Concentrations on April 30 were higher than normal but considerably less than observed. The ability of the CTM to capture the high ^{7}Be concentrations on these days is encouraging. High ^{7}Be concentrations in the upper troposphere are usually associated with air that has recently been in the stratosphere. It appears that the location and time of major STE events are captured by the UMD−CTM when driven by GEOS−3 DAS fields. The magnitude of most events is underestimated possibly due to the relatively coarse resolution of the model.

Mean model−calculated and observed ^{7}Be profiles in the southern (latitudes < 60°N) and northern (latitudes > 60°) portions of the TOPSE region are shown in Figures 3a−b, respectively. The profiles were obtained by sorting individual ^{7}Be measurements and model output interpolated to the same location as a function of pressure. The solid (derived from observations) and dashed (derived from model output) lines show weighted least squares third order polynomial fits to the sorted fields. The sampling periods were used as weights. Fits to the trop−^{7}Be component are shown with pluses. Measurements show a "S−like" ^{7}Be profile with concentration maxima in the upper and lower troposphere. This "S−like" feature is fairly well

captured by the model in the northern portion of the TOPSE region but is barely evident in the southern portion of the TOPSE region.

Excessive cross−tropopause flux has been a problem with CTMs driven by data from the GEOS DAS [*Liu et al*., 2001; *Bey et al*., 2001], but it does not appear to be a significant problem in this simulation. Model−calculated mean upper tropospheric concentrations exceed measured concentrations by 10 ± 15%. The magnitude of cross tropopause flux can also be evaluated by comparing the stratospheric component of model−calculated ^{7}Be with estimates of the component derived using atmospheric measurements [*Liu et al*., 2001]. The stratospheric component of model−calculated ^{7}Be in a model layer is calculated by dividing the strat−^{7}Be concentration by the total ^{7}Be concentration. Observation−based estimates of the stratospheric component utilize ^{90}Sr and ^{7}Be data. ^{90}Sr is a long−lived radionucleide produced by nuclear detonations and lost by scavenging in the troposphere. An estimate of the strat−^{7}Be concentration in the troposphere can be obtained by multiplying ^{90}Sr concentrations in the troposphere by ^{7}Be/ ^{90}Sr ratios in the lower stratosphere [*Dutkiewicz and Husain*, 1985]. This estimate is an upper bound since it assumes that the ^{7}Be/ ^{90}Sr ratio is preserved in the troposphere (i.e., it ignores changes in the ratio due to decay of ^{7}Be). The stratospheric component is obtained by dividing the resulting strat−^{7}Be concentrations by measured ^{7}Be concentrations in the troposphere. Analyses of lower stratospheric ^{7}Be/ ^{90}Sr ratios from samples taken during NASA's Global Atmospheric Sampling Program (GASP) and ground−level ^{7}Be and ^{90}Sr measurements at Environmental Measurement Laboratory (EML) sites (38° − 51° N) indicate that the stratospheric component of ^{7}Be in the surface layer increased from 25 to 38% during the February to May period [*Dutkiewicz and Husain*, 1985]. The stratospheric component for this latitude band in the lowest layer of the UMD−CTM during the February to May period increased from 39 to 42%. This bias suggests that cross tropopause flux in the UMD−CTM when driven

by GEOS−3 DAS fields is too high by 35 ± 20%. This value is 25% higher than the estimate derived by comparing upper tropospheric profiles. Which value is likely to be most accurate?

Model−calculated lower tropospheric concentrations in the southern portion of the TOPSE region are up to a factor of two too small. A possible cause is excessive wet scavenging in the UMD−CTM. The precipitation rate and the liquid water content determine scavenging rates in the UMD−CTM. Precipitation rates appear to be reasonable. Monthly average GEOS−3 DAS precipitation rates for the 100°−60° W, 30°−60° N region during the TOPSE period differ from satellite−gauge precipitation estimates from the Global Precipitation Climatology Project Version 2 Combined Precipitation Data Set [*Huffman et al*., 1995; *Susskind et al*., 1997] by less than 20%. Within this region, precipitation rates are underestimated north of 40° N, especially during February and overestimated south of 40°N, especially during May. An estimate of the liquid water content is not available from the GEOS−3 DAS. We followed *Giorgi and Chameides* [1986] and assumed a cloud condensed water content of 0.5×10^{-3} kg m^{-3} when calculating the fraction of a grid volume experiencing large−scale convection. This value may be appropriate for highly soluble gases and aerosols but overestimates the scavenging of ^{7}Be, especially at higher latitudes [*Brost et al*., 1991]. An overestimation of scavenging would result in an overestimation of the stratospheric component because trop−^{7}Be is preferentially scavenged (see section 5). Therefore, the bias derived using ^{7}Be/ ^{90}Sr ratios is likely to be an upper bound on the cross tropopause flux bias. We suspect cross tropopause flux is overestimated in the UMD−CTM when driven by GEOS−3 DAS fields, but only by 10−25%. Strat−^{7}Be is not constrained in the following simulations.

This small bias is a dramatic improvement over the biases seen in earlier simulations driven by the GEOS DAS. Stratosphere−troposphere exchange was overestimated by a factor of 3 when the distributions of ^{7}Be and O_3 were simulated using 2° x 2.5° sigma layer CTMs driven

by GEOS DAS fields [*Liu et al.*, 2001; *Bey et al.*, 2001]. The calculations discussed in this paper were driven by a more recent version of the GEOS DAS; however, the main difference between these and the previous simulations is the vertical grid. A sigma−pressure coordinate system was used for these simulations while a sigma coordinate system was used for the previous calculations.

The variability of observed and model−calculated concentrations as a function of pressure is shown in Figures 3c−d, respectively. The variation of standard deviation with pressure was estimated by fitting a third order polynomial to the standard deviations of concentrations in seven different pressure bins (see Table 2). Model−calculated concentrations are less variable than observed, especially in the upper troposphere. The underestimation is at least partially due to the 2° x 2.5° resolution of the model. The magnitude of variability in a 1° x 1° simulation that is still being analyzed is more realistic. Both the measurements and model output show a peak in variability in the upper troposphere. Measurements also show a variability minimum in the mid−troposphere near 600 hPa. The model does not captures this minimum. The variation of the model−calculated stratospheric component with pressure at the location of TOPSE measurements is shown in Figure 3e. It equals 25% near the surface and increases gradually to 40% at 600 hPa. It then increases rapidly and is greater than 70% by 350 hPa.

The method of least squares was used to fit a regression line to the change with time of ^{7}Be concentrations in four pressure bins in the southern and northern portions of the TOPSE region (see Tables 3 and 4). No clear trends were present. The statistically significant (at a 95% confidence interval (CI)) increase in the mid−troposphere (500−650 hPa) in the northern portion of the region can be discounted because sampling pressures in this bin decreased significantly with time. Statistically insignificant but interesting temporal changes can be seen at sampling

pressures of less than 500 hPa. Temporal changes at these pressures appear to differ between the southern and northern portions of the TOPSE region. Observed and model−calculated concentrations increase with time in the southern portion of the region and decrease with time in the northern portion of the region. The changes are not caused by a "trend" in the sampling altitude. Mean upper tropospheric sampling pressures in both regions increase by only 4−5 hPa per month.

Five−minute averaged O_3 concentrations in the southern portion of the TOPSE region increased significantly (at a 99% CI) with time in each of the four pressure bins (Table 5). Five−minute averaged O_3 concentrations in the northern portion of the TOPSE region increased significantly at the same CI in the mid−tropospheric layers (425−650 hPa) but showed no trend in the uppermost and lowermost layers. The different ^{7}Be and O_3 "trends" is a strike against the hypothesis that seasonal differences in STE control seasonal differences in O_3. A more definite conclusion is not possible with this type of analysis because sampling conditions (synoptic situation, pressure, duration, and location) varied greatly from day−to−day and even sample−to−sample during the TOPSE period. A more extensive discussion of O_3 trends during TOPSE is given in *Browell et al*. [this issue].

In an effort to determine if the stratospheric component at the longitude and latitude of the TOPSE measurements is representative of the entire TOPSE region, probability distribution functions (PDFs) of the stratospheric component on the flight dates in the upper− (~392 hPa) and middle− (~682 hPa) troposphere are shown in Figure 4. Mean stratospheric components at the location of TOPSE measurements differ only slightly from mean stratospheric components for the region in general. It appears that model output at the location of TOPSE measurements is representative of the TOPSE region.

4.2. Individual flights

The variation of ^{7}Be concentrations within flights 12 (February 25), 16 (March 7), 28 (April 7), and 35 (April 28) will now be investigated in more detail. The February 25, April 7, and April 28 flights originated in Thule and ended in Churchill. The March 7 flight began and ended in Churchill. Model−calculated and observed ^{7}Be concentrations as a function of time are shown in Figures 5a−d. Model−calculated and observed ^{7}Be concentrations track well. Within each flight, concentrations show a strong dependence on pressure; although considerable variation is also seen during several constant altitude segments (e.g., 18−21 UT February 25 and 14−15 UT March 7). The model does a reasonable job of capturing this constant altitude variation. Periods when analysis of temporal fluctuations in ^{7}Be, O_3, and HNO_3 data indicated that stratospheric influence was large are shown with X's [*Dibb et al*., this issue]. Both model−calculated and observed concentrations are enhanced during these periods; although, model−calculated concentrations are usually too low. The underestimation of variability is not surprising. Model−calculated concentrations were obtained by interpolating 2° x 2.5° model output at 00, 06, 12, and 18 UT to the measurement location and time. Sampling periods were only 10−20 minutes which translates to 75−150 km (½ − 1 grid box) at typical C−130 speeds.

Curtain plots for each of the four flights are shown in Figures 6a−d. The location of the GEOS−3 DAS tropopause is shown by triangles. The gradient between the uppermost troposphere and the lower stratosphere is striking! Clearly, ^{7}Be is a sensitive tracer of STE. From comparison of ^{7}Be measurements and model output it appears that the location of tropopause folds is reasonably well simulated by the model. It is also interesting to note that the 18 UT February 25 and 16:30 UT April 7 measurements were taken in relative ^{7}Be minima.

5. Evaluation of stratospheric input to the troposphere

The first step in determining the stratospheric input to the troposphere was to determine the mass of ^{7}Be in the troposphere. The tropospheric ^{7}Be mass was calculated for each 2° x 2.5° column by summing the mass of ^{7}Be in each tropospheric model layer. Model layers were assumed to be tropospheric if they were entirely within the troposphere. The tropopause was determined using GEOS−3 DAS tropopause pressures. The mean tropospheric ^{7}Be concentrations in the southern and northern portions of the TOPSE regions were calculated by dividing the total ^{7}Be mass within each region by the total mass of air in each region. Variations with time of mean tropospheric model−calculated ^{7}Be concentrations in the southern and northern portions of the TOPSE region are shown in Figures 7a−b, respectively. Concentrations increase by 2.9% per month in the southern portion of the region and 1.6% per month in the northern portion of the region. Both trop−^{7}Be and strat−^{7}Be increase with time; although, the relative increase of each component varies between the southern and northern portion of the TOPSE region. Trop−^{7}Be concentrations increase by 2.0% in the southern portion of the region and by 2.4% in the northern portion of the region. Strat−^{7}Be concentrations increase by 3.5% in the southern region but by only 0.9% in the northern region. Consequently, the stratospheric component in the southern portion of the TOPSE region increases by 0.57% per month, while the stratospheric component in the northern portion of the TOPSE region decreases by 0.69% per month (Figures 7c−d).

Interpretation of these percentage increases and decreases is complicated by the fact that changes in the rates of several processes contribute to the increases and decreases in tropospheric ^{7}Be concentrations and stratospheric components. A balance between four processes controls seasonal variations in tropospheric ^{7}Be concentrations [*Feely et al.*, 1989]. These processes are

STE, vertical mixing within the troposphere, meridional transport within the troposphere, and scavenging. The relative importance of each of these processes depends on location and season. The relative importance of each of these processes in the TOPSE regions was analyzed using budgets constructed from UMD−CTM output. Changes in the tropospheric mass of trop−^{7}Be and strat−^{7}Be in the southern (Figure 8) and northern (Figure 9) portions of the TOPSE region due to some of these processes will now be examined.

Temporal changes in tropospheric ^{7}Be mass (the sum of trop−^{7}Be and strat−^{7}Be) due to temporal changes in scavenging are shown in Figures 8a and 9a. The importance of ^{7}Be loss due to scavenging varies by more than a factor of 6 (after adjusting for area) between the southern and northern portions of the TOPSE region. Losses due to scavenging increase rapidly with time especially in the southern portion of the TOPSE region. The increase in scavenging with time increases the stratospheric component of ^{7}Be because scavenging is largest in the lower portions of the troposphere where concentrations of trop−^{7}Be exceed concentrations of strat−^{7}Be. The stratospheric components of scavenged ^{7}Be in the southern and northern portions of the TOPSE region were 39.4 and 42.9%, respectively. These percentages are considerably less than the mean stratospheric component of atmospheric ^{7}Be in the troposphere in each of these regions, 60.5 and 57.1%, respectively.

Temporal changes in tropospheric ^{7}Be mass due to temporal changes in chemistry are shown in Figures 8b and 9b. Since the rates of ^{7}Be production and decay were held fixed throughout the simulation, these time series reflect changes in the mean tropospheric height with time. Since total ^{7}Be production within the troposphere exceeds loss by decay, the mean change is positive. A small increase with time is evident due to seasonal changes in the tropopause pressure. Changes in the mass of tropospheric ^{7}Be due to changes in net ^{7}Be production (production − decay) with time are relatively small when compared to changes due to other

processes (compare slopes of changes). Net ^{7}Be production by this mechanism increases slightly with time in the southern portion of the TOPSE region but is nearly unchanged in the northern portion of the TOPSE region.

Temporal changes in ^{7}Be mass within the troposphere due to mass convergence are shown for trop−^{7}Be in Figures 8c and 9c and for strat−^{7}Be in Figures 8d and 9d. The mass convergence term includes changes in ^{7}Be mass due to advection as well as changes in ^{7}Be mass due to changes in background mass (surface pressure). Convergence over the entire TOPSE period results in a net loss of trop−^{7}Be. This ^{7}Be may be lost to the stratosphere via isentropic transport across the tropopause or diabatic ascent or to regions outside of the TOPSE domain via horizontal transport within the troposphere. The rate of loss decreases with time in both TOPSE regions. Convergence results in a net increase of strat−^{7}Be. The increase is much larger in the southern portion of the TOPSE region than in the northern portion. Strat−^{7}Be enters the TOPSE region via STE within the TOPSE region or via horizontal advection following STE at locations outside of the TOPSE region. The increase in the convergence of strat−^{7}Be with time requires that STE also increase with time. The increase in convergence will lag the increase in STE unless the exchange occurs over the TOPSE region.

The changes in the budget terms with time can be used to interpret the changes in the stratospheric component shown in Figures 7c−d. The stratospheric component in the southern portion of the TOPSE region increases with time due to temporal increases in scavenging and STE. Increases in scavenging increase the stratospheric component because trop−^{7}Be is preferentially scavenged. Increases in STE increase the component because the increase in strat−^{7}Be due to convergence (mostly STE) exceeds the increase in trop−^{7}Be due to convergence. The overall increase of the component is only 0.6% per month. An increase of this magnitude would result in tropospheric O_3 increases of only 1% per month. This back of the envelope calculation

assumes stratospheric O_3 concentrations exceed tropospheric O_3 concentrations by a factor of 10 and an initial stratospheric component of 55%. The stratospheric component in the northern portion of the TOPSE region decreases with time because increases in the component due to an increase in scavenging are more than balanced by decreases in the component due to the preferential convergence of trop−^{7}Be via meridional advection into the northern portion of the TOPSE region. The effect of STE on the northern portion of the TOPSE region does not appear to increase with time.

6. Summary

A primary goal of TOPSE was to determine the causes of a springtime tropospheric O_3 maxima over mid− to high−latitude continental North America. Measurements of ^{7}Be, a tracer of stratospheric air, were taken during the TOPSE mission. The distribution of ^{7}Be during the TOPSE period was also calculated using a 35 sigma−pressure layer 2° x 2.5° version of the UMD−CTM driven by data from the GEOS−3 DAS. The ^{7}Be source function was divided into tropospheric and stratospheric components, and separate simulations were performed for ^{7}Be with a tropospheric (trop−^{7}Be) and a stratospheric (strat−^{7}Be) source. Model−calculated and observed ^{7}Be concentrations were analyzed in an attempt to determine if the stratospheric component of tropospheric air in the TOPSE region increased with time during the spring. Seasonal changes in the stratospheric component of tropospheric air are a possible cause of the observed O_3 maxima.

Comparison of model−calculated ^{7}Be concentrations with measurements revealed that cross tropopause exchange of ^{7}Be was overestimated but only by 10−25%. This bias is much less than what was seen in earlier calculations driven by the GEOS DAS. The main difference

between these and earlier simulations is the vertical coordinate of the CTM. These calculations were run using a sigma−pressure coordinate system while the previous calculations were run using a sigma coordinate system. In general, temporal fluctuations in ^{7}Be concentrations were well captured even during constant altitude portions of TOPSE flights, although the magnitudes of the fluctuations were usually underestimated. Mean observed ^{7}Be profiles in the southern and northern portion of the TOPSE region are "S−like" in shape. This "S−like" structure is fairly well captured by the model in the northern part of the TOPSE region but barely evident in the southern portion of the TOPSE region. The stratospheric component of ^{7}Be in air sampled during the TOPSE mission appears to be representative of the TOPSE region in general. Within the TOPSE region [100°−60°W, 40°−80°N], 55−60% of ^{7}Be in the model troposphere had a stratospheric source, and 25−35% of ^{7}Be in the surface layer had a stratospheric source.

Mid− and upper−tropospheric O_3 concentrations increase significantly with time during the TOPSE period. A similar increase with time of ^{7}Be might be expected if seasonal changes in STE controlled seasonal changes in tropospheric O_3 concentrations. However, ^{7}Be measurements were quite variable and no significant increase was found during the TOPSE period.

Model−calculated mean tropospheric ^{7}Be concentrations increased by 2.9% per month in the southern portion [100°−60°W, 40°−60°N] of the TOPSE region. The increase is consistent with statistically insignificant increases seen in upper−tropospheric ^{7}Be data from TOPSE. Both trop−^{7}Be and strat−^{7}Be increased with time. The stratospheric component increased by only 0.6% per month. Analysis of the ^{7}Be budget shows that seasonal increases in STE and scavenging contribute to this increase. Tropospheric O_3 increases resulting from this increase in STE are likely to be less than 1% per month.

Model−calculated mean tropospheric ^{7}Be concentrations increased by 1.6% per month in

the northern portion [100°−60°W, 60°−80°N] of the TOPSE region. ^{7}Be measurements do not show an increase during this time period. Analysis of the ^{7}Be budget showed that seasonal increases in STE did not contribute to this increase. Changes in this region appear to be due to the preferential convergence of trop−^{7}Be via meridional advection into the northern portion of the TOPSE region.

Appendix

Beryllium−7 concentrations are expressed in milli−Becquerels per cubic meter at standard temperature and pressure (mBq/SCM) or fento−Curies per SCM (fCi/SCM) where 1 mBq/SCM equals 27 fCi/SCM. The ^{7}Be source used in this study was expressed in atoms of ^{7}Be per gram of air per second (atoms ^{7}Be g^{-1} s^{-1}). The resulting concentrations were in atoms ^{7}Be g^{-1}. A Becquerel is defined as a disintegration per second. The disintegration rate of ^{7}Be (d^{7}Be/dt) is given by −^{7}Be/tau where tau is the lifetime (76.88*86400s). The density at STP equals 1.293 kg m^{-3}. The concentration in Bq/SCM is obtained by multiplying the concentration in atoms ^{7}Be g−1 by the density and dividing by the lifetime. One Bq/SCM equals 1000 mBq/SCM. Therefore one mBq/SCM equals 0.1947 atoms ^{7}Be g^{-1}.

Acknowledgments: The authors would like to thank Dorothy Koch for providing the ^{7}Be source distribution that was used in this paper, Louise Emmons for creating the TOPSE data merges, and Luca Cinquini for managing the many TOPSE data sets and presentations. This research is supported under NSF Grant ATM9910210.

References

Allen, D. J., R. B. Rood, A. M. Thompson, and R. D. Hudson, Three−dimensional radon−222 calculations using assimilated meteorological data and a convective mixing algorithm, *J. Geophys. Res.*, 101, 6871−6881, 1996a.

Allen, D. J., P. Kasibhatla, A. M. Thompson, R. B. Rood, B. G. Doddridge, K. E. Pickering, R. D. Hudson, and S. −J. Lin, Transport−induced interannual variability of carbon monoxide determined using a chemistry and transport model, *J. Geophys. Res*, 101, 28,655−28,669, 1996b.

Appenzeller, C., J. R. Holton, and K. H. Rosenlof, Seasonal variation of mass transport across the tropopause, *J. Geophys. Res*., 101, 15,071−15,078, 1996.

Arakawa, A., and W. H. Schubert, Interaction of a cumulus cloud ensemble with the large−scale environment, Part I, *J. Atmos. Sci.*, 31, 674−701, 1974.

Bazhanov, V., and H. Rodhe, Tropospheric ozone at the Swedish mountain site Areskutan: budget and trends, *J. Atmos. Chem*., 28, 61−76, 1997.

Bey, I., D. J. Jacob, R. M. Yantosca, J. A. Logan, B. D. Field, A. M. Fiore, Q. Li, H. Y. Liu, L. J. Mickley, and M. G. Schultz, Global modeling of tropospheric chemistry with assimilated meteorology: Model description and evaluation, *J. Geophys. Res*., 106, 23,073−23,095, 2001.

Bloom, S. C., L. L. Takacs, A. M. DaSilva, and D. Ledvine, Data assimilation using incremental

analysis updates, *Mon. Weather Rev.*, 124, 1256−1271, 1996.

Brasseur, G. P., D. A. Hauglustaine, S. Walters, P. J. Rasch, J.−F. Müller, L. K. Emmons, and M. A. Carroll, MOZART, a global chemical transport model for ozone and related chemical tracers, 1, Model description, *J. Geophys. Res.*, 103, 28,265−28,289, 1998.

Brost, R. A., J. Feichter, and M. Heimann, Three−dimensional simulation of Be−7 in a global climate model, *J. Geophys. Res.*, 96, 22,423−22,445, 1991.

Browell, E. W., et al., Ozone, aerosol, potential vorticity, and trace gas trends observed at high latitudes from February to May 2000 over North America, *J. Geophys. Res.*, this issue.

Chin, M., R. B. Rood, S. −J. Lin, J.−F. Müller, and A. M. Thompson, Atmospheric sulfur cycle simulated in the global model GOCART: Model description and global properties, *J. Geophys. Res.*, 105, 24,671−24,687, 2000.

Cooper, O. R., J. L. Moody, J. C. Davenport, S. J. Oltmans, B. J. Johnson, X. Chen, P. B. Shepson, and J. T. Merrill, Influence of springtime weather systems on vertical ozone distributions over three North American sites, *J. Geophys. Res.*, 103, 22,001−22,013, 1998.

Danielson, E. F., Stratospheric−tropospheric exchange based upon radioactivity, ozone, and potential vorticity, *J. Atmos. Sci.*, 25, 502−518, 1968.

Dibb, J. E., R. W. Talbot, and G. L. Gregory, Beryllium 7 and Lead 210 in the Western

Hemisphere Arctic Atmosphere: Observations From Three Recent Aircraft−Based Sampling Programs, *J. Geophys. Res*., 97, 16,709−16,715, 1992.

Dibb, J., E., L. D. Meeker, R. C. Finkel, J. R. Southon, M. W. Caffee, and L. A. Barrie, Estimation of stratospheric input to the Arctic troposphere: 7−Be and 10−Be in aerosols, at Alert, Canada, *J. Geophys. Res*., 99, 12,855−12,864, 1994.

J. E. Dibb, R. W. Talbot, Seid, Scheuer, DeBell, B. Ridley, and Lefer, Stratospheric Influence on the Northern North American Free Troposphere During TOPSE: Be−7 as a Stratospheric Tracer, *J. Geophys. Res*., this issue, 2001.

Dutkiewicz, V. A., and L. Husain, Stratospheric and tropospheric components of ^{7}Be in surface air, *J. Geophys. Res.*, 90, 5783−5788, 1985.

Feely, H. W., R. J. Larsen, and C. G. Sanderson, Factors That Cause Seasonal Variations in Beryllium−7 Concentrations in Surface Air, *J. Environ. Radioactivity*, 9, 223−249, 1989.

Giorgi, F., and W. L. Chameides, Rainout lifetimes of highly soluble aerosols and gases as inferred from simulations with a general circulation model, *J. Geophys. Res.*, 91, 14,367−14,376, 1986.

Holton, J. R., P.H. Haynes, M. E. McIntyre, A. R. Douglass, R. B. Rood, and L. Pfister, *Rev. Geophys*., 33, 403−439, 1995.

Huffman, G. J., R. F. Adler, B. Rudolf, U. Schneider, and P. R. Keehn, Global precipitation estimates based on a technique for combining satellite−based estimates, rain gauge analysis, and NWP model precipitation information, *J. Climate*, 8, 1284−1295, 1995.

Husain, L. P. E. Coffey, R. E. Meyers, and R. T. Cederwall, Ozone transport from stratosphere to troposphere, *Geophys. Res. Letts.*, 4, 363−365, 1977.

Koch, D., and D. Rind, Beryllium 10/beryllium 7 as a tracer of stratospheric transport, *J. Geophys. Res.*, 103, 3907−3917, 1998.

Koch, D., D. J. Jacob, and W. C. Graustein, Vertical transport of tropospheric aerosols as indicated by ^{7}Be and ^{210}Pb in a chemical tracer model, *J. Geophys. Res.*, 101, 18,651−18,666, 1996.

Lal, D., On the investigations of geophysical processes using cosmic ray produced radioactivity, in *Earth Science and Meteoritics*, compiled by J. Geiss and E. D. Goldberg, 312 pp., North−Holland, New York, 1963.

Lal, D., and B. Peters, Cosmic ray produced radioactivity on the Earth, in *Handbuch der Physik*, 46/2, 551−612, edited by K. Sitte, Springer−Verlag, New York, 1967.

Lawrence, M. G., and P. J. Crutzen, The impact of cloud particle gravitational settling on soluble trace gas distributions, *Tellus*, 50B, 263−289, 1998.

Lin, S. −J., and R. B. Rood, Multidimensional flux form semi−Lagrangian transport schemes, *Mon. Weather Rev.*, 124, 2046−2070, 1996.

Liu, H., D. J. Jacob, I. Bey, and R. M. Yantosca, Constraints from ^{210}Pb and ^{7}Be on wet deposition and transport in a global three−dimensional chemical tracer model driven by assimilated meteorological fields, *J. Geophys. Res.*, 106, 12,109−12,128, 2001.

Logan, J. A., Tropospheric ozone: Seasonal behavior, trends, and anthropogenic influence, *J. Geophys. Res.*, 90, 10,463−10,482, 1985.

Moody, J. L., J. C. Davenport, J. T. Merrill, S. J. Oltmans, D. D. Parrish, J. S. Holloway, H. Levy II, G. L. Forbes, M. Trainer, and M. Buhr, Meteorological mechanisms for transporting O_3 over the western North Atlantic Ocean: A case study for August 24−29, 1993, *J. Geophys. Res.*, 101, 29,213−29,227, 1996.

Moorthi, S., and M. J. Suarez, Relaxed Arakawa−Schubert: A parameterization of moist convection for general circulation models, *Mon. Weather Rev.*, 120, 978−1002, 1992.

Oltmans, S. J., Surface ozone measurements in clean air, *J. Geophys. Res.*, 86, 1174−1180, 1981.

Penkett, S. A., and K. A. Brice, The spring maximum in photo−oxidants in the Northern Hemisphere troposphere and lower stratosphere, *Nature*, 319, 655−675, 1986.

Postel, G. A., and M. H. Hitchman, A climatology of Rossby wave breaking along the subtropical tropopause, *J. Atmos. Sci*., 359−373, 1999.

Rehfeld, S., and M. Heimann, Three dimensional atmospheric transport simulation of the radioactive tracers ^{210}Pb, ^{7}Be, ^{10}Be, and ^{90}Sr, *J. Geophys. Res.*, 100, 26,141−26,161, 1995.

Ridley, B., et al., Ozone depletion events observed in the high latitude surface layer during the TOPSE aircraft program, *J. Geophys. Res*., this issue.

Sander, R., and P. J. Crutzen, Model study indicating halogen activation and ozone destruction in polluted air masses transported to the sea, *J. Geophys. Res.*, 101, 9121−9138, 1996.

Schubert, S. D., R. B. Rood, and J. Pfaendtner, An assimilated data set for earth science applications, *Bull. Am. Meteorol. Soc.*, 74, 2331−2342, 1993.

Susskind, J., P. Piraino, L. Rokke, L. Iredell, and A. Mehta, Characteristics of the TOVS Pathfinder Path A Dataset, *Bull. Amer. Meteor. Soc*., 78, 1449−1472, 1997.

Viezee, W., and H. B. Singh, The distribution of beryllium−7 in the troposphere: Implications on stratospheric/tropospheric air exchange, *Geophys. Res. Letts*., 7, 805−808, 1980.

Figures

1. Zonally averaged mean (February 1 − May 31, 2000) model−calculated ^{7}Be as a function of latitude and pressure. a) Concentration in units of 1, 2, 5, 7.5, 10, 15, 20, 50, 100, 200, and 350 mBq/SCM, b) Percent with a stratospheric source. Contour intervals of 20, 25, 30, 35, 40, 50, 60, 70, 80, and 90%.

2. Model−calculated vs. measured ^{7}Be concentration (mBq / SCM) as a function of flight date. The component of model−calculated ^{7}Be with a tropospheric (stratospheric) source is shown with diagonal (horizontal) lines. The mean sampling pressure of the aircraft is shown with "P's". The mean tropopause pressure is shown with "T's".

3. ^{7}Be profiles constructed using TOPSE measurements and model output interpolated to the same location and time. a) measured−^{7}Be (solid), model−calculated total−^{7}Be (dashed), and model−calculated trop−^{7}Be (bold +'s) for sampling latitudes of ≤ 60°N, b) Same as a) but for sampling latitudes of >60°N, c) UNH ^{7}Be data at all latitudes ± 1σ, d) model−calculated total−^{7}Be at all latitudes ± 1σ. e) Percent of model−calculated ^{7}Be with a stratospheric origin ± 1σ.

4. Probability density functions of the stratospheric component of ^{7}Be in the UMD−CTM. The solid line shows a PDF of model output at the location and time of the TOPSE measurements. The dotted lines show PDFs from 18 UT model output for the same day. These PDFs are for the same longitude and latitude as the measurements but at ~392 (upper) and ~682 (lower) hPa. The dashed lines show PDFs from 18 UT model output for the same day for the TOPSE region [100°−60°W, 40°−80°N] at ~392 (upper) and ~682 (lower) hPa.

5. Model−calculated vs. measured ^{7}Be on a) 25 February, b) 7 March, c) 7 April, and d) 28 April. Measured concentrations are shown with boxes. The hatched (shaded) region shows the contribution of model−calculated ^{7}Be with a tropospheric (stratospheric) source. A solid line shows the mean sampling pressure. Time periods when stratospheric influence is believed to be large are shown with an X.

6. Curtain plots comparing model−calculated ^{7}Be concentrations above and below the flight paths. Measured concentrations are proportional to asterisk size and range from 0.9 to 113.0 mBq/SCM. Sampling pressures are given by the lowest points on each of the asterisks. Dates shown are a) 25 February, b) 7 March, c) 7 April, and d) 28 April. GEOS−3 DAS tropopause pressures are shown with triangles.

7. Time series of mean model−calculated tropospheric ^{7}Be in the southern (7a) and northern (7b) portions of the TOPSE region. The solid lines show total ^{7}Be concentrations. The dashed and dotted lines show the contribution from strat−^{7}Be and trop−^{7}Be, respectively. Mean stratospheric components in the troposphere for the southern and northern portions of the TOPSE region are shown in Figures 7c and 7d, respectively.

8. Processes affecting tropospheric ^{7}Be concentrations within the southern portion of the TOPSE region. a) Mass of scavenged ^{7}Be (trop−^{7}Be + strat−^{7}Be) as a function of time, b) Net change in ^{7}Be mass (trop−^{7}Be + strat−^{7}Be) due to production and decay, c) Net change in trop−^{7}Be mass due to mass convergence by advection and/or changes in the surface pressure, d) Same as c but for strat−^{7}Be mass. In order to reduce noise, a boxcar smoother of width 30 was applied to the 5 February to 27 May mass convergence fields before plotting. Least square fits to each of the terms before smoothing are shown with straight lines. Units for the changes are mBq/SCM * kg*1.e−15.

9) Same as 8 but for northern portion of TOPSE region.

Table 1. Monthly average global and TOPSE region (100°−60°W, 40°−80°N) ^{7}Be budget for trop−^{7}Be and strat−^{7}Be. Units are g /month and percent as appropriate.

GLOBAL BUDGET

	Trop−^{7}Be		Strat−^{7}Be	
	Mass	Loss(%)	Mass	Loss(%)
Source	3.61		8.69	
Decay	0.90	24.6%	6.75	81.6%
Wet dep	2.63	72.3%	1.45	17.6%
Dry dep	0.11	3.1%	0.07	0.9%

TOPSE REGION BUDGET

	Trop−^{7}Be		Strat−^{7}Be	
	Mass	Loss(%)	Mass	Loss(%)
Source	0.065		0.355	
Decay	0.018	35.4%	0.251	90.9%
Wet dep	0.029	58.4%	0.023	8.5%
Dry dep	0.003	6.2%	0.002	0.6%

Table 2. Statistics for ^{7}Be data and model output at the same location after binning data and model output into 7 pressure bins. Pressures (hPa) at the top and bottom of each bin are given by P(top) and P(bot), respectively. The number of data points in each bin is given by Npts. Mean concentrations (mBq/SCM) and standard deviations are given in the "mean" and "stddev" columns.

TOPSE measurements

P(top)	P(bot)	Npts	mean	stddev
350	400	60	40.50	44.94
400	500	126	19.09	18.95
500	600	40	12.93	10.12
600	700	20	12.47	10.08
700	800	10	9.68	13.05
800	900	20	8.56	6.56
900	1021	22	2.55	1.85

Total−^{7}Be (model)

P(top)	P(bot)	Npts	mean	stddev
350	400	60	36.52	17.24
400	500	126	22.01	9.60
500	600	40	14.88	7.18
600	700	20	8.38	4.01
700	800	10	7.76	4.87
800	900	20	5.30	2.55
900	1021	22	1.04	0.67

Table 3. Statistics for ^{7}Be data and model output at the same location after binning into 4 pressure bins. Only data and model output collected at latitudes equatorward of 60°N are included. Pressures at the top and bottom of each bin are given by P(top) and P(bot), respectively. The number of data points in each bin is given by Npts. Mean concentrations (mBq/SCM) and standard deviations are given in the "mean" and "stddev" columns. The trend (mBq/SCM per month) and 95% confidence intervals for it are given in the "Min, Mean, and Max" columns.

			TOPSE measurements				
P(top)	P(bot)	Npts	mean	stddev	Min	Mean	Max
350	425	55	33.63	42.09	−2.00	8.37	18.73
425	500	47	16.62	13.56	−3.06	0.56	4.18
500	650	14	11.27	10.75	−6.89	−1.67	3.55
650	1021	29	9.27	10.46	−3.56	−0.05	3.47

			Total−^{7}Be (model)				
P(top)	P(bot)	Npts	mean	stddev	Min	Mean	Max
350	425	55	30.54	14.11	−1.40	2.11	5.63
425	500	47	18.34	9.09	−0.82	1.57	3.95
500	650	14	11.46	7.62	−5.18	−1.53	2.13
650	1021	29	5.12	4.28	−0.35	1.03	2.41

Table 4. Same as table 3 but for sampling latitudes poleward of 60°N.

			TOPSE measurements				
P(top)	P(bot)	Npts	mean	stddev	Min	Mean	Max
350	425	20	43.32	40.68	−34.63	−12.47	9.69
425	500	64	20.91	22.57	−6.68	−1.03	4.63
500	650	30	13.03	9.61	−0.05	3.38	6.82
650	1021	39	7.01	7.55	−2.02	0.53	3.08

			Total−^{7}Be (model)				
P(top)	P(bot)	Npts	mean	stddev	Min	Mean	Max
350	425	20	46.35	17.28	−13.63	−4.07	5.49
425	500	64	23.37	8.77	−1.41	0.78	2.98
500	650	30	15.58	6.75	0.66	2.98	5.29
650	1021	39	4.96	4.26	−0.33	1.06	2.46

Table 5. Statistics for O_3 data from the 5−minute merge product at latitudes equatorward and poleward of 60°N. Pressures at the top and bottom of each bin are given by P(top) and P(bot), respectively. The number of data points in each bin is given by Npts. Mean concentrations (ppbv) and standard deviations are given in the "mean" and "stddev" columns. The trend (ppbv per month) and 99% confidence intervals for it are given in the "Min, Mean, and Max" columns.

Sampling latitudes less than 60°N

P(top)	P(bot)	Npts	mean	stddev	Min	Mean	Max
350	425	276	76.32	41.14	9.48	14.83	20.19
425	500	303	61.43	19.94	4.39	6.73	9.07
500	650	207	57.44	11.84	0.31	2.23	4.14
650	1021	391	47.86	11.28	0.99	2.33	3.67

Sampling latitudes greater than 60°N

P(top)	P(bot)	Npts	mean	stddev	Min	Mean	Max
350	425	112	88.05	29.33	−8.16	0.20	8.55
425	500	345	68.39	13.05	5.92	7.40	8.88
500	650	202	64.24	10.04	6.36	7.60	8.83
650	1021	345	42.53	17.63	−2.30	0.10	2.50

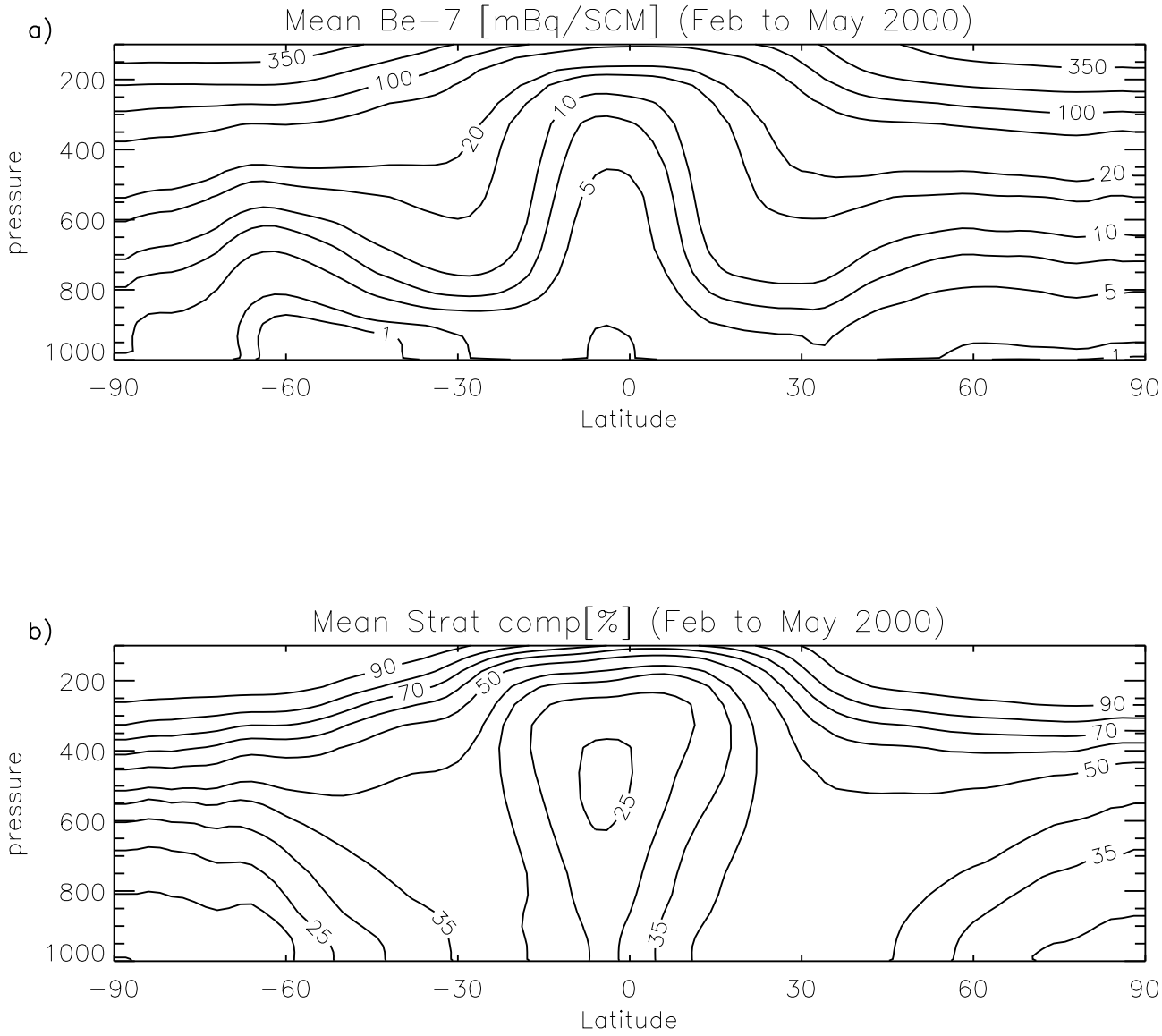
a)
Mean Be−7 [mBq/SCM] (Feb to May 2000)
pressure
200
400
600
800
1000
350
100
20
10
5
1
−90
−60
−30
0
30
60
90
Latitude
b)
Mean Strat comp[%] (Feb to May 2000)
pressure
90
70
50
25
35
Latitude

Figure 1

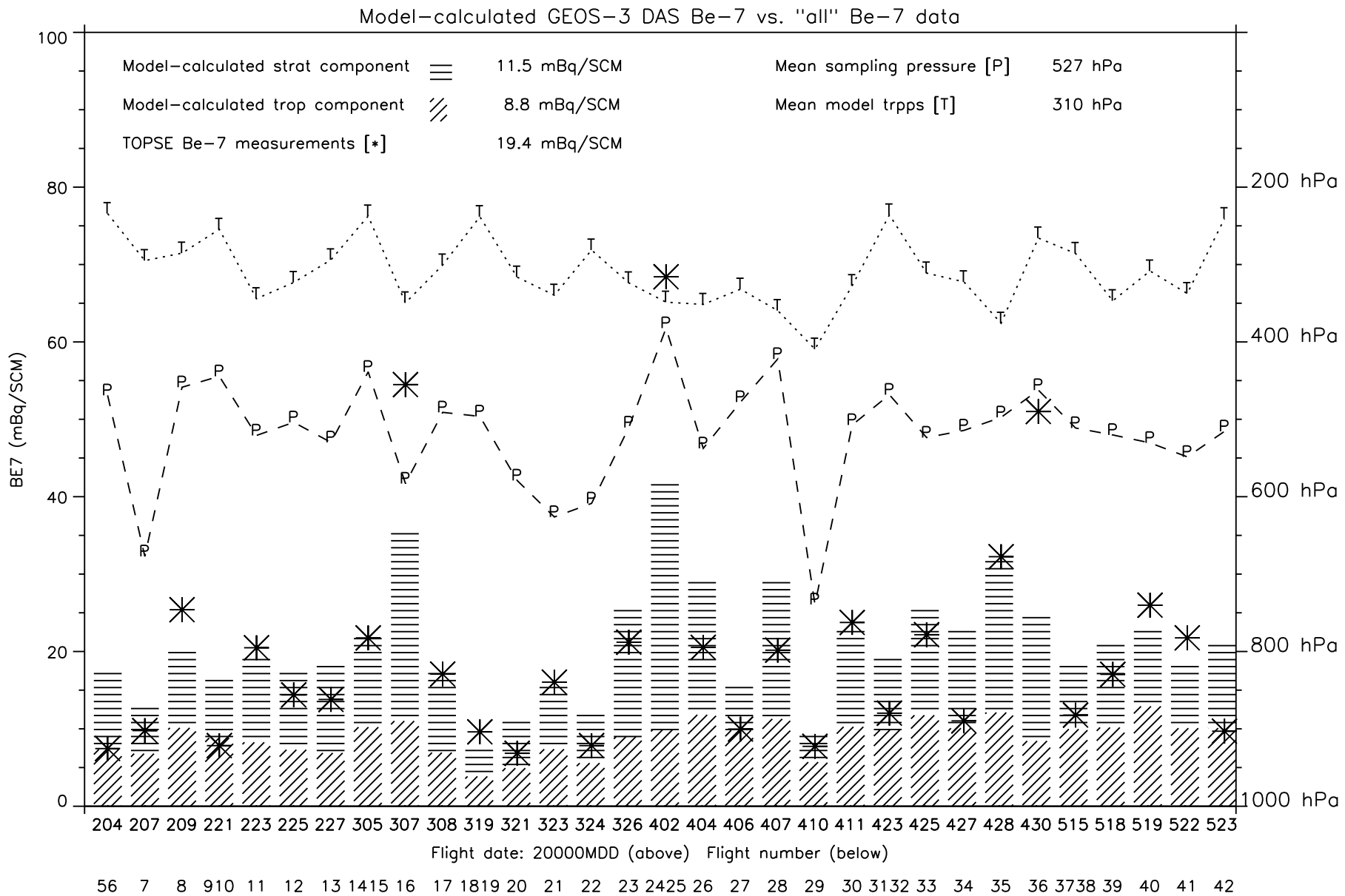
Model−calculated GEOS−3 DAS Be−7 vs. "all" Be−7 data
Model−calculated strat component 11.5 mBq/SCM
Model−calculated trop component 8.8 mBq/SCM
TOPSE Be−7 measurements [*] 19.4 mBq/SCM
Mean sampling pressure [P] 527 hPa
Mean model trpps [T] 310 hPa
BE7 (mBq/SCM)
100
80
60
40
20
0
200 hPa
400 hPa
600 hPa
800 hPa
1000 hPa
204 207 209 221 223 225 227 305 307 308 319 321 323 324 326 402 404 406 407 410 411 423 425 427 428 430 515 518 519 522 523
Flight date: 20000MDD (above) Flight number (below)
56 7 8 910 11 12 13 1415 16 17 1819 20 21 22 23 2425 26 27 28 29 30 3132 33 34 35 36 3738 39 40 41 42

Figure 2

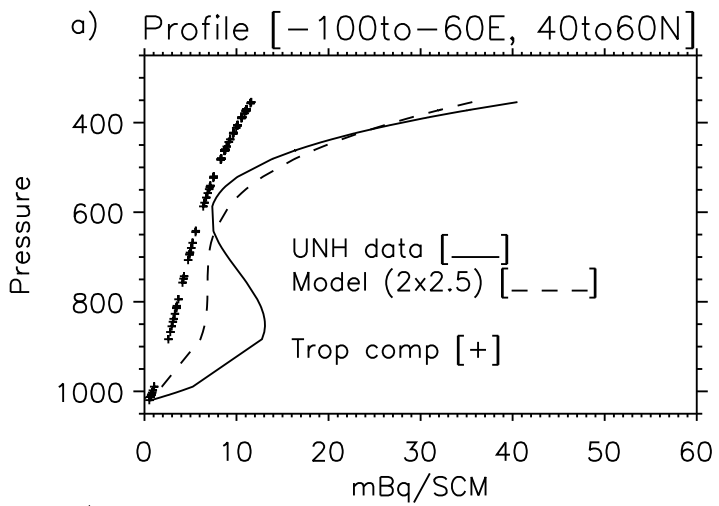
a) Profile [−100to−60E, 40to60N]
Pressure
400
600
800
1000
0
10
20
30
40
50
60
mBq/SCM
UNH data [___]
Model (2x2.5) [_ _ _]
Trop comp [+]

Figure 3

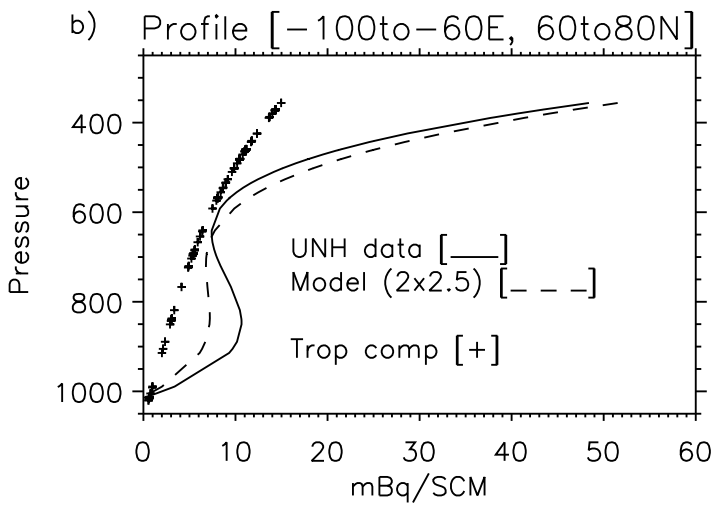
b) Profile [−100to−60E, 60to80N]
Pressure
400
600
800
1000
0
10
20
30
40
50
60
mBq/SCM
UNH data [___]
Model (2x2.5) [_ _ _]
Trop comp [+]

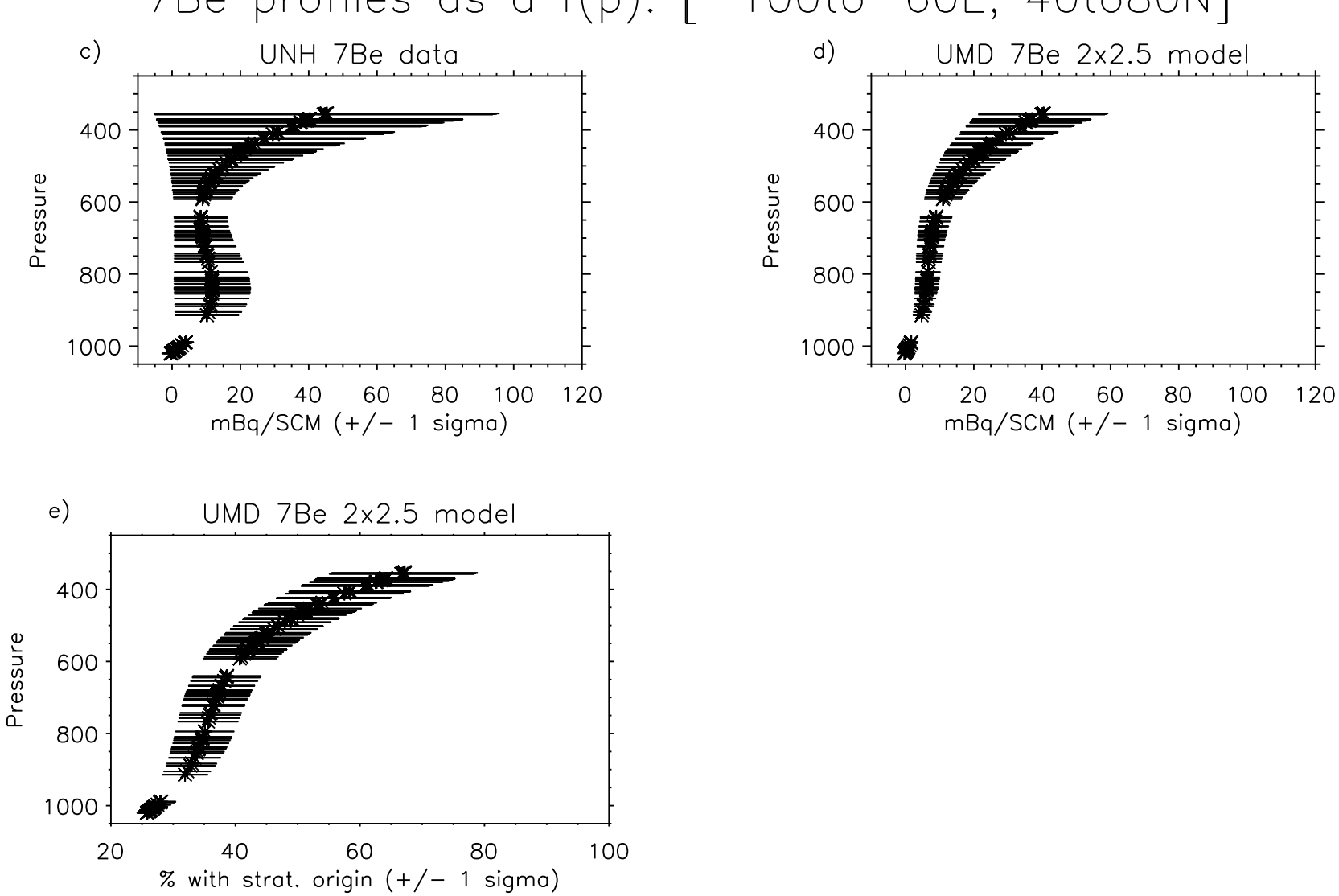
7Be profiles as a f(p): [−100to−60E, 40to80N]
c)
UNH 7Be data
d)
UMD 7Be 2x2.5 model
e)
UMD 7Be 2x2.5 model
Pressure
400
600
800
1000
0
20
40
60
80
100
120
mBq/SCM (+/− 1 sigma)
% with strat. origin (+/− 1 sigma)

Figure 3

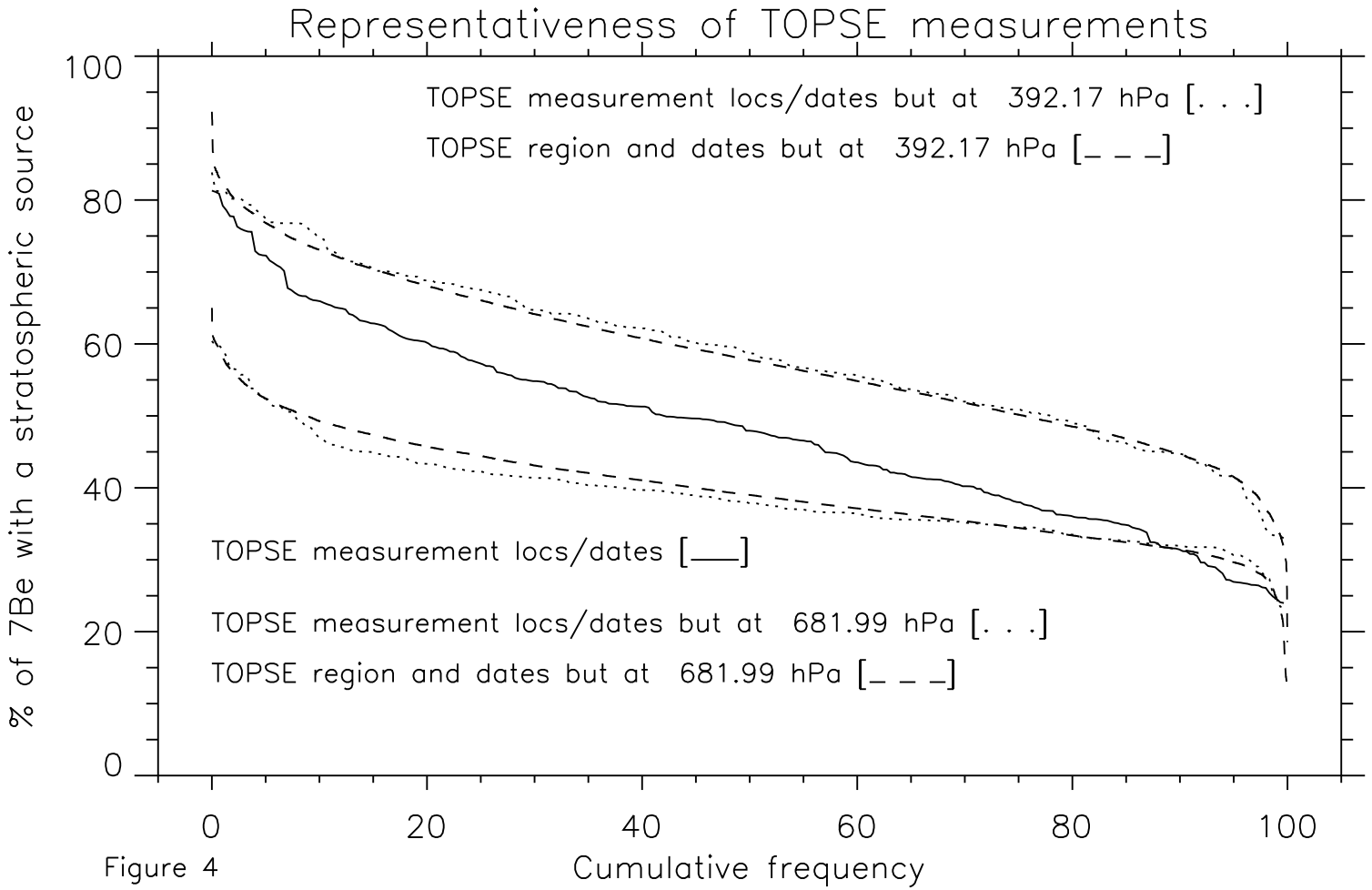
Representativeness of TOPSE measurements
TOPSE measurement locs/dates but at 392.17 hPa [. . .]
TOPSE region and dates but at 392.17 hPa [_ _ _]
TOPSE measurement locs/dates [___]
TOPSE measurement locs/dates but at 681.99 hPa [. . .]
TOPSE region and dates but at 681.99 hPa [_ _ _]
% of 7Be with a stratospheric source
Cumulative frequency
0
20
40
60
80
100

Figure 4

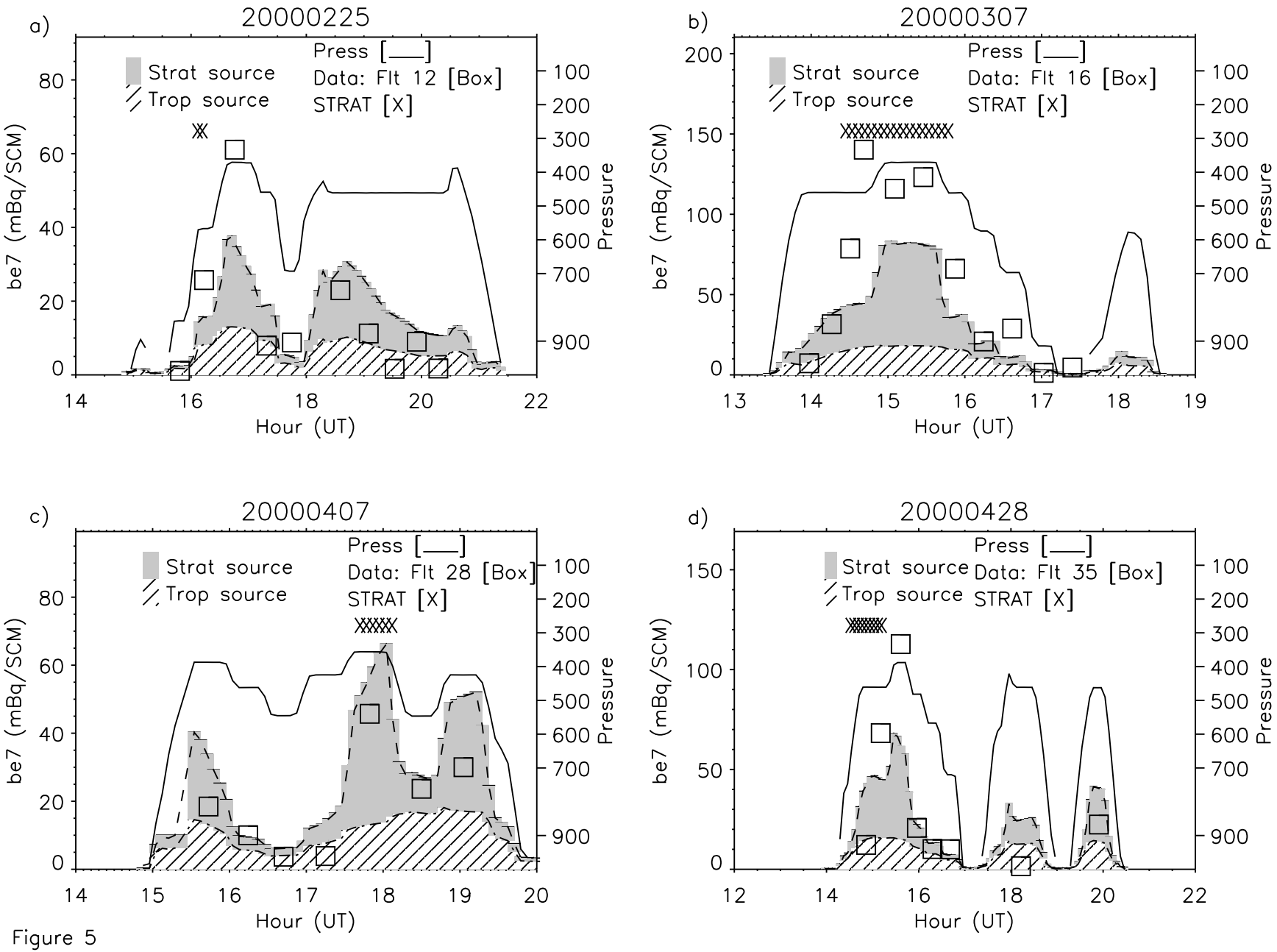
a)
20000225
Press [___]
Data: Flt 12 [Box]
STRAT [X]
Strat source
Trop source
be7 (mBq/SCM)
Pressure
Hour (UT)
b)
20000307
Press [___]
Data: Flt 16 [Box]
STRAT [X]
Strat source
Trop source
be7 (mBq/SCM)
Pressure
Hour (UT)
c)
20000407
Press [___]
Data: Flt 28 [Box]
STRAT [X]
Strat source
Trop source
be7 (mBq/SCM)
Pressure
Hour (UT)
d)
20000428
Press [___]
Data: Flt 35 [Box]
STRAT [X]
Strat source
Trop source
be7 (mBq/SCM)
Pressure
Hour (UT)

Figure 5

UMD/GEOS-3 7Be (2x2.5 UG)

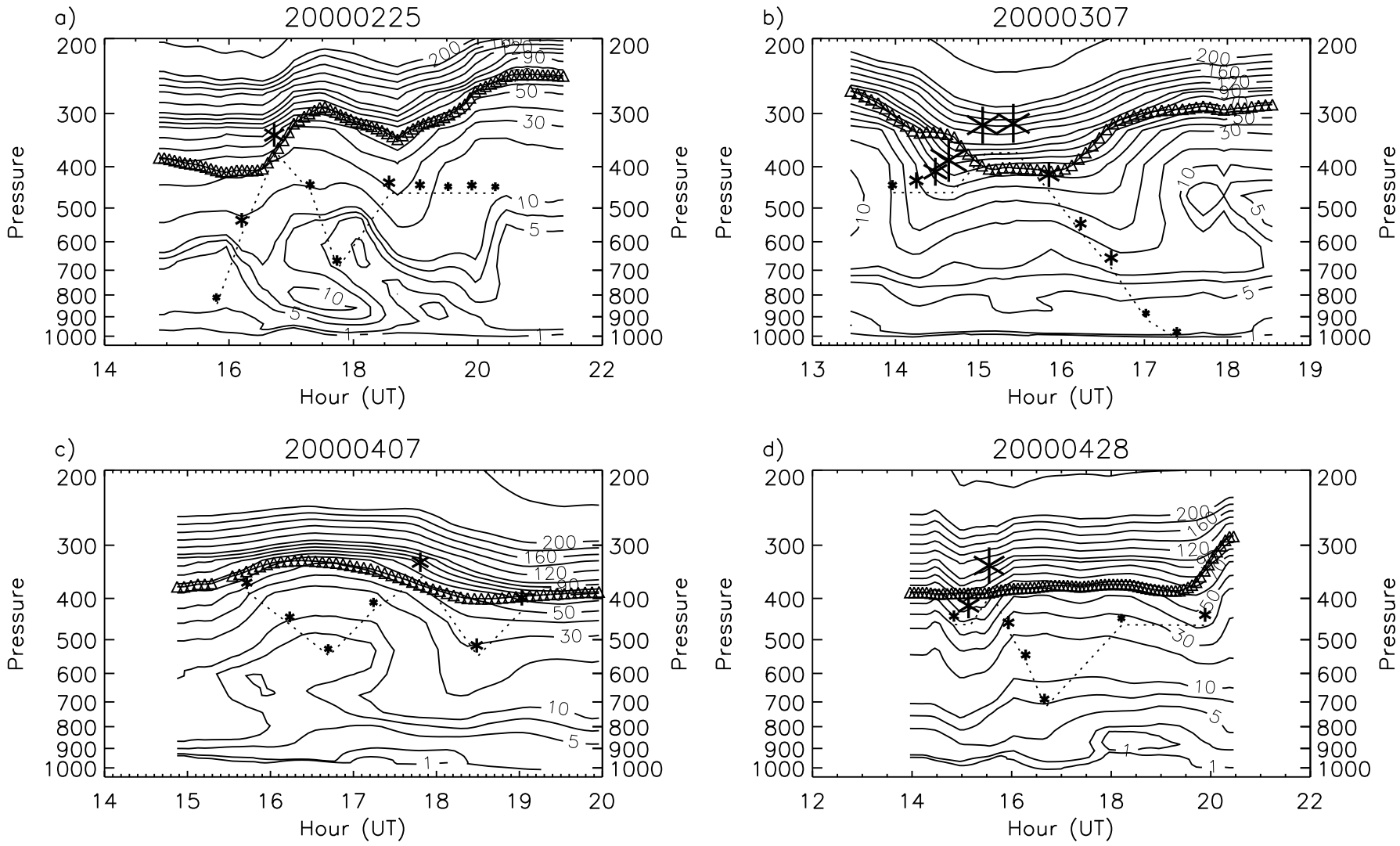

Figure 6

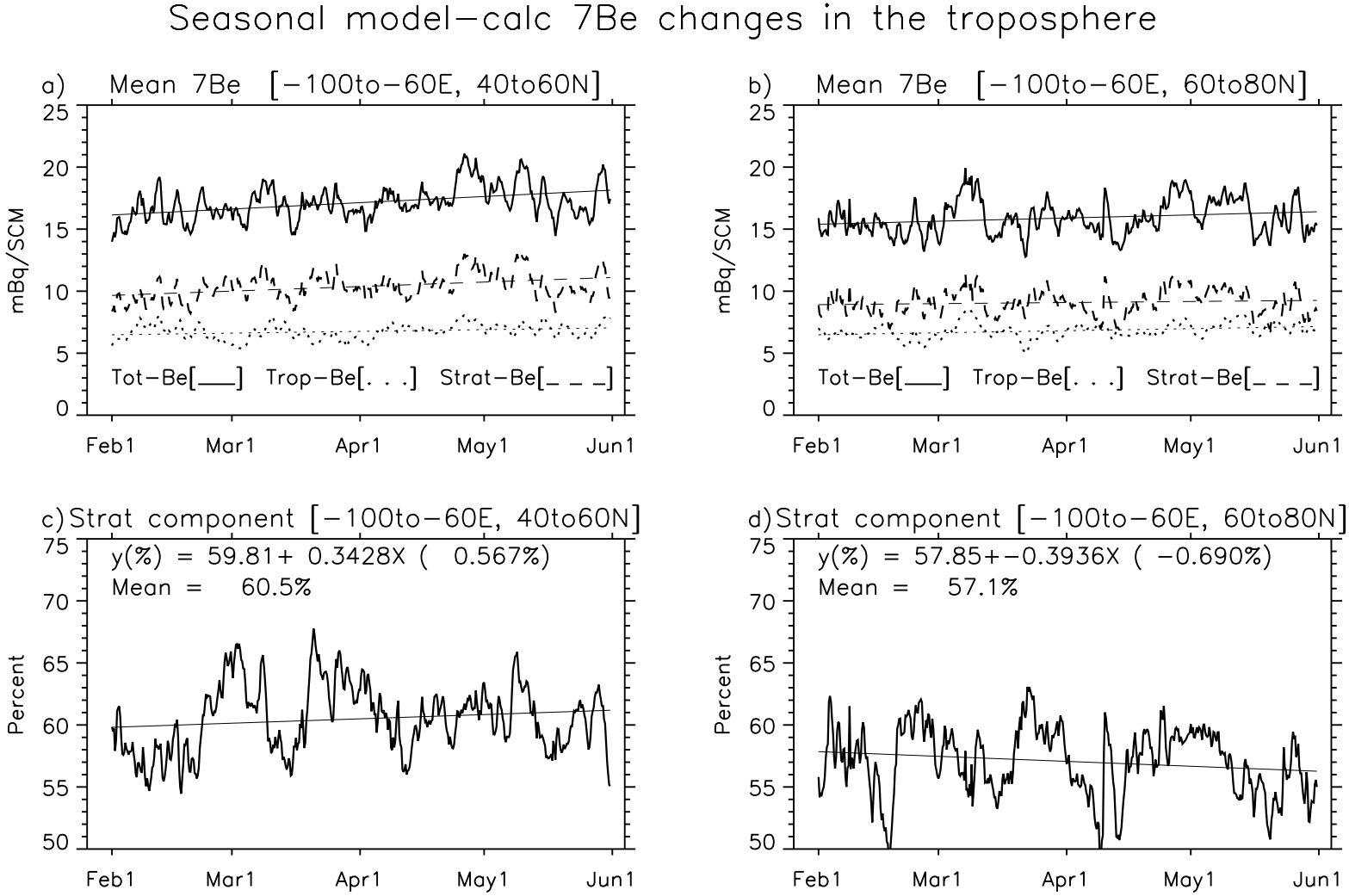
Seasonal model−calc 7Be changes in the troposphere
a) Mean 7Be [−100to−60E, 40to60N]
b) Mean 7Be [−100to−60E, 60to80N]
mBq/SCM
Tot−Be[___] Trop−Be[. . .] Strat−Be[_ _ _]
Feb1
Mar1
Apr1
May1
Jun1
c) Strat component [−100to−60E, 40to60N]
d) Strat component [−100to−60E, 60to80N]
y(%) = 59.81+ 0.3428X (0.567%)
Mean = 60.5%
y(%) = 57.85+−0.3936X (−0.690%)
Mean = 57.1%
Percent

Figure 7

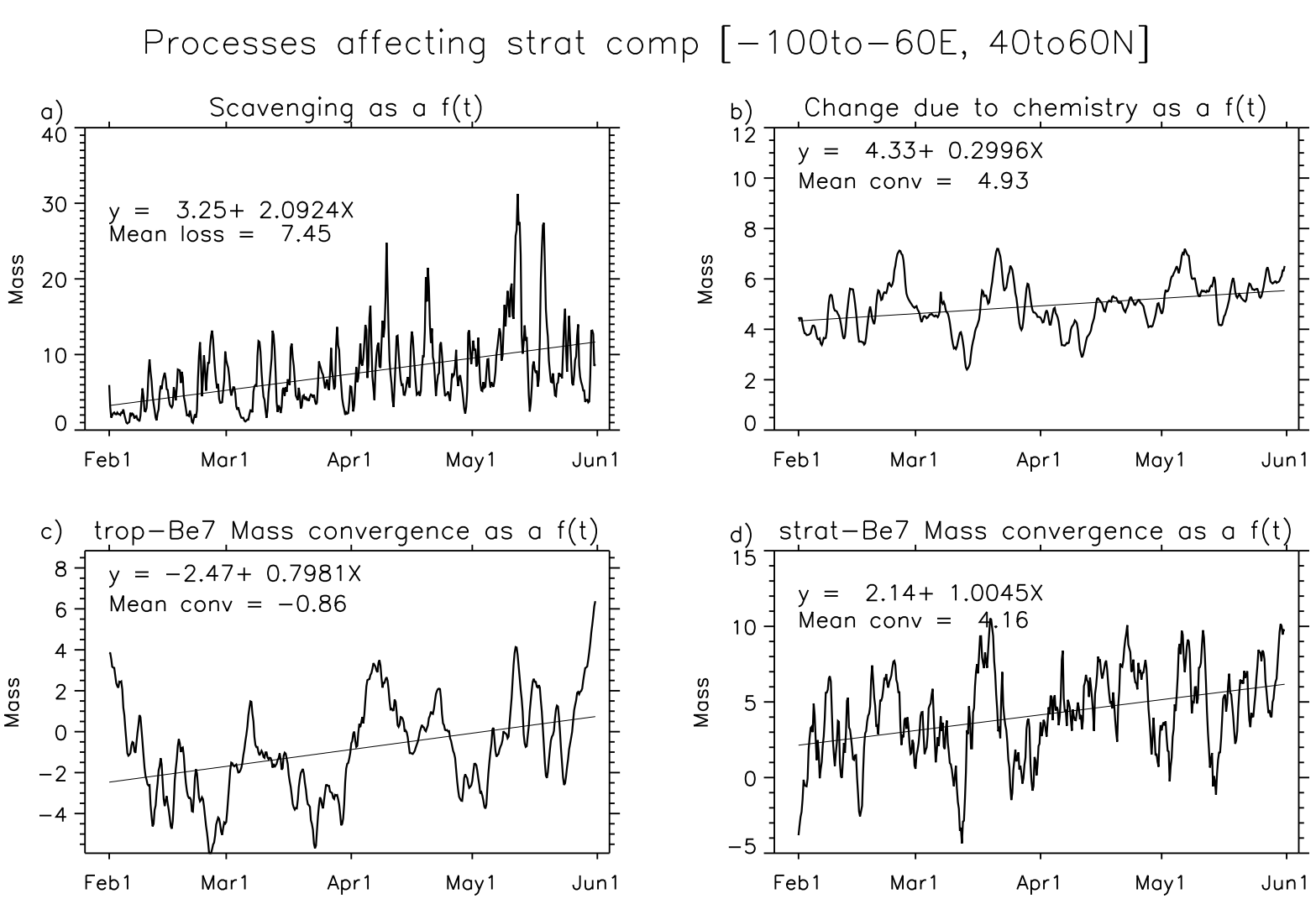
Processes affecting strat comp [−100to−60E, 40to60N]
a) Scavenging as a f(t)
y = 3.25+ 2.0924X
Mean loss = 7.45
b) Change due to chemistry as a f(t)
y = 4.33+ 0.2996X
Mean conv = 4.93
c) trop−Be7 Mass convergence as a f(t)
y = −2.47+ 0.7981X
Mean conv = −0.86
d) strat−Be7 Mass convergence as a f(t)
y = 2.14+ 1.0045X
Mean conv = 4.16
Mass
Feb1
Mar1
Apr1
May1
Jun1

Figure 8

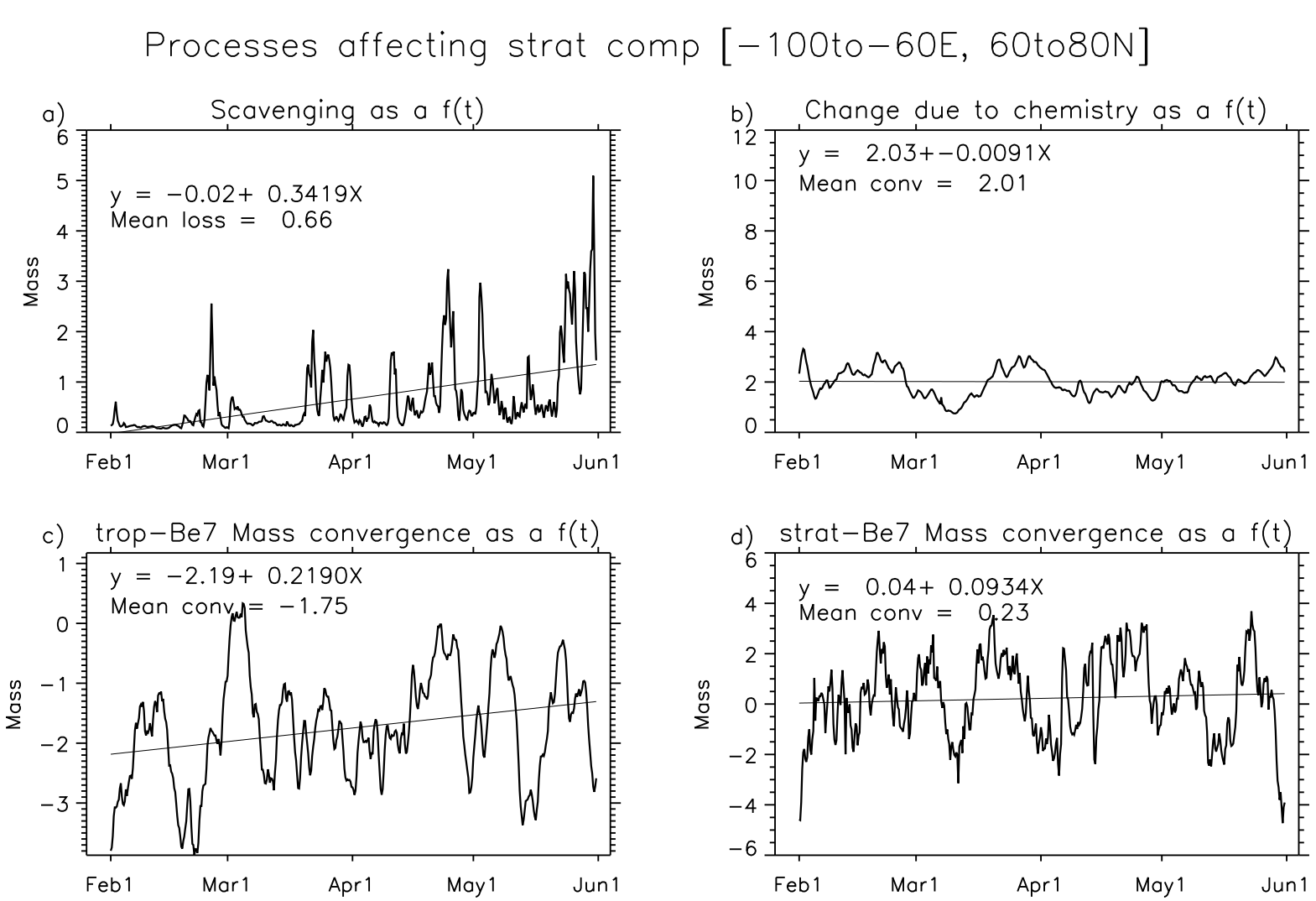
Processes affecting strat comp [−100to−60E, 60to80N]
a) Scavenging as a f(t)
y = −0.02+ 0.3419X
Mean loss = 0.66
b) Change due to chemistry as a f(t)
y = 2.03+−0.0091X
Mean conv = 2.01
c) trop−Be7 Mass convergence as a f(t)
y = −2.19+ 0.2190X
Mean conv = −1.75
d) strat−Be7 Mass convergence as a f(t)
y = 0.04+ 0.0934X
Mean conv = 0.23
Mass
Feb1
Mar1
Apr1
May1
Jun1

Figure 9